Mon. Not. R. Astron. Soc. **384,** 1003–1014 (2008) doi:10.1111/j.1365-2966.2007.12773.x

Radio circular polarization produced in helical magnetic fields in eight active galactic nuclei

D. C. Gabuzda,[1⋆] V. M. Vitrishchak,[2] M. Mahmud[1] and S. P. O'Sullivan[1]

[1]*Physics Department, University College Cork, Cork, Ireland*
[2]*Sternberg Astronomical Institute, Moscow State University, Universitetskiu prospekt 13, Moscow 119992, Russia*

Accepted 2007 November 23. Received 2007 November 23; in original form 2007 February 23

ABSTRACT

Homan & Lister have recently published circular polarization (CP) detections for 34 objects in the MOJAVE sample – a set of bright, compact active galactic nuclei (AGN) being monitored by the Very Long Baseline Array at 15 GHz. We report the detection of 15-GHz parsec-scale CP in two more AGN (3C 345 and 2231+114), and confirm the MOJAVE detection of CP in 1633+382. It is generally believed that the most likely mechanism for the generation of this CP is Faraday conversion of linear polarization (LP) to CP. A helical jet magnetic field (***B*** field) geometry can facilitate this process – linearly polarized emission from the far side of the jet is converted to CP as it passes through the magnetized plasma at the front side of the jet on its way towards the observer. In this case, the sign of the generated CP is essentially determined by the pitch angle and helicity of the helical ***B*** field. We have determined the pitch-angle regimes and helicities of the helical jet ***B*** fields in eight AGN for which parsec-scale CP has been detected, and used them to predict the expected CP signs for these AGN if the CP is generated via conversion in these helical fields. We have obtained the intriguing result that our predictions agree with the observed signs in all eight cases, provided that the longitudinal ***B*** field components in the jets correspond to south magnetic poles. This clearly non-random pattern demonstrates that the observed CP in AGN is directly associated with the presence of helical jet ***B*** fields. These results suggest that helical ***B*** fields are ubiquitous in AGN jets.

Key words: galaxies: active – galaxies: jets – quasars: general.

1 INTRODUCTION

The radio emission of core-dominated, radio-loud active galactic nuclei (AGN) is synchrotron radiation generated in the relativistic jets that emerge from the nucleus of the Galaxy, presumably along the rotational axis of a central supermassive black hole. Synchrotron radiation can be highly linearly polarized, to $\simeq$75 per cent in the case of a uniform magnetic (***B***) field (Pacholczyk 1970), and LP observations can yield unique information about the orientation and degree of the order of the ***B*** field in the synchrotron source as well as the distribution of thermal electrons and the ***B*** field geometry in the immediate vicinity of the AGN (e.g. via Faraday rotation of the plane of polarization).

After a number of early circular polarization (CP) studies for various samples of AGN in the 1970s and 1980s (Gilbert & Conway 1970; Conway et al. 1971; Roberts et al. 1975; Weiler & Wilson 1977; Weiler & de Pater 1983; Komesaroff et al. 1984), little observational work was done in this area until the late 1990s, when the Australia Telescope Compact Array was optimized for CP measurements by Rayner, Norris & Sault (2000), and techniques for deriving CP information on parsec scales were developed by Homan and his collaborators (Homan & Wardle 1999; Homan, Attridge & Wardle 2001) using the NRAO[1] Very Long Baseline Array (VLBA). The high resolution provided by these latter observations makes it possible to more precisely localize the regions of CP within the source, and thereby more accurately estimate the degree of CP in these regions. Certain tendencies became clear from the very first VLBA CP measurements: the CP was nearly always coincident with the very long baseline interferometry (VLBI) core, with the degrees of CP typically being tenths of a per cent. Comparisons with integrated data obtained earlier indicated that the sign of the CP for a given source usually remained constant on time-scales of decades. In addition, it became clear that CP could occasionally be detected in compact components in the inner VLBI jets.

CP measurements of AGN have recently made another major step forward with the publication of first-epoch CP results for the 133 sources in the MOJAVE sample of radio-bright AGN, which

⋆E-mail: gabuzda@phys.ucc.ie

[1] The National Radio Astronomy Observatory of the USA is operated by Associated Universities, Inc., under cooperative agreement with the US NSF.

are regularly monitored by the VLBA at 15 GHz (Homan & Lister 2006). Of these sources, 34 displayed CP at the positions of their total-intensity peaks (nearly always the VLBI core) at a level of 2σ or greater, with the typical degrees of CP being a few tenths of a per cent. Comparison with 20 different optical, radio and intrinsic parameters of the AGN yielded virtually no evidence for any correlation between the degree of CP and these other parameters. Another exciting result of the first-epoch MOJAVE CP measurements was that five of the sample sources clearly displayed appreciable CP in their VLBI *jets*, well resolved from the core, indicating that a CP-generation mechanism capable of operating effectively in optically thin regions was involved.

We consider here the hypothesis that the parsec-scale CP is generated via Faraday conversion in helical jet $\boldsymbol{B}$ fields in these AGN, focusing on the *sign* of the observed CP, which has not been investigated in previous studies. We first examine the sign of CP generated by Faraday conversion (Section 2), then turn to the special case of conversion in a helical magnetic field geometry (Section 3). In Section 3, we also describe our approach for using multifrequency VLBI polarization data to determine the expected CP sign for particular AGN in a simple helical jet $\boldsymbol{B}$-field model. Sections 4 and 5 discuss the data used for our analysis and our results: new detections of CP and transverse jet Faraday-rotation gradients in several AGN, and our remarkable result that the CP signs expected in our simple model agree with the observed signs in all eight AGN for which the comparison was possible, provided their longitudinal $\boldsymbol{B}$ field components correspond to south poles. The robustness and implications of this result are discussed in Section 6, and our conclusions summarized in Section 7.

2 THE SIGN OF CIRCULAR POLARIZATION GENERATED BY CONVERSION

Various possible mechanisms for the generation of CP in relativistic astrophysical jets are discussed, for example, by Macquart & Melrose (2000), Wardle & Homan (2002, 2003), Beckert & Falcke (2002) and Ensslin (2003). Incoherent synchrotron radiation produces a very small amount of CP at frequencies of several to tens of gigahertz (Legg & Westfold 1968), and the observed degrees of CP are high enough to make this mechanism implausible. A much more likely mechanism is the Faraday conversion of LP to CP during propagation through a magnetized plasma (Jones & O'Dell 1977; Jones 1988); although this mechanism has been studied fairly extensively theoretically and demonstrated to be plausible, the action of Faraday conversion has not been directly demonstrated observationally.

In order for Faraday conversion to operate, the observed LP electric ($\boldsymbol{E}$) vector must have non-zero components both parallel and perpendicular to the $\boldsymbol{B}$ field in the conversion region projected on to the sky, $\boldsymbol{B}_{\rm conv}$. We will describe this electric vector using components parallel to $\boldsymbol{B}_{\rm conv}$, $\boldsymbol{E}_{\parallel}$, and orthogonal to $\boldsymbol{B}_{\rm conv}$, $\boldsymbol{E}_{\perp}$. $\boldsymbol{E}_{\parallel}$ excites oscillations of free charges in the plasma, while $\boldsymbol{E}_{\perp}$ cannot, since the charges are not free to move perpendicular to $\boldsymbol{B}_{\rm conv}$. This leads to a delay between $\boldsymbol{E}_{\parallel}$ and $\boldsymbol{E}_{\perp}$, manifests as the introduction of a small amount of CP; the sign of the CP depends on the relative phase of $\boldsymbol{E}_{\parallel}$ and $\boldsymbol{E}_{\perp}$. Unlike Faraday rotation, Faraday conversion does not depend on the sign of the free charges involved. A full mathematical description of Faraday conversion is given by Jones & O'Dell (1977); we will be concerned here only with a qualitative understanding of the origin of the *sign* of CP generated by Faraday conversion in a simple $\boldsymbol{B}$ field geometry.

To demonstrate the sign of the CP that arises due to Faraday conversion, we consider a foreground (conversion) field $\boldsymbol{B}_{\rm conv}$, which purely for convenience of illustration (to avoid our diagrams from becoming overly cluttered) we take to lie in the y direction on the sky (Fig. 1), in a right-handed 'observer's' coordinate system in which north (the x direction) is upward and east (the y direction) is to the left-hand side. We suppose that LP is generated in an optically thin background synchrotron source, and that the conversion delays correspond to phase shifts of less than 90°. In this case, the key parameter determining the sign of the resulting CP turns out to be the angle Φ between the synchrotron $\boldsymbol{B}$ field, $\boldsymbol{B}_{\rm gen}$ and $\boldsymbol{B}_{\rm conv}$,

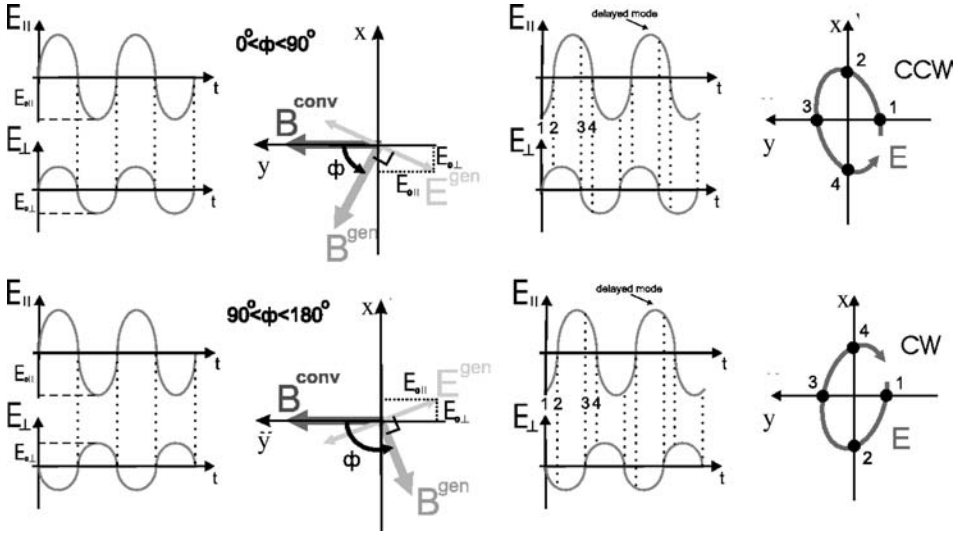

Figure 1. Partial conversion of LP from synchrotron radiation generated in a background field $\boldsymbol{B}_{\rm gen}$ to CP in a foreground field $\boldsymbol{B}_{\rm conv}$ for the case when the angle Φ between the two fields projected on to the sky is between 0° and 90° (top) and between 90° and 180° (bottom). From left- to right-hand side, the plots show the relationship between the oscillations of $\boldsymbol{E}_{\parallel}$ and $\boldsymbol{E}_{\perp}$ of the synchrotron polarization $\boldsymbol{E}$ vector parallel and perpendicular to $\boldsymbol{B}_{\rm conv}$; the relationship between $\boldsymbol{B}_{conv}$, $\boldsymbol{B}_{\rm gen}$ and $\boldsymbol{E}_{\rm gen}$ on the sky; and the resulting CP that arises when $\boldsymbol{E}_{\parallel}$ is delayed with respect to $\boldsymbol{E}_{\perp}$. The points labelled 1, 2, 3, 4 refer to successive times. The total $\boldsymbol{E}$ vector rotates in the CCW direction (+ CP, or right-hand CP) when $0° > \Phi > 90°$ and in the CW direction (− CP, or left-hand CP) when $90° > \Phi > 180°$.

projected on to the plane of the sky, measured in the usual sense from north through east, as shown (Fig. 1). The observed LP $\boldsymbol{E}$ vector will be orthogonal to $\boldsymbol{B}_{\rm gen}$, since the synchrotron emission region is optically thin.

In principle, some amount of conversion is inevitable if Φ differs from 0° (180°) and 90° (270°). The angle Φ lies in one of the four quadrants (i) $0^\circ < \Phi < 90^\circ$, (ii) $90^\circ < \Phi < 180^\circ$, (iii) $180^\circ < \Phi < 270^\circ$ or (iv) $270^\circ < \Phi < 360^\circ$. As examples, Fig. 1 qualitatively illustrates the connection between the angle Φ, the resulting delay between $\boldsymbol{E}_\parallel$ and $\boldsymbol{E}_\perp$ and the sign of the resulting CP for the first two cases. In case (i), the oscillations of $\boldsymbol{E}_\parallel$ and $\boldsymbol{E}_\perp$ are in phase (they have the same sign), and the tip of the vector sum of $\boldsymbol{E}_\parallel$ and $\boldsymbol{E}_\perp$ moves in the counterclockwise (CCW) direction on the sky, corresponding to positive CP (right-hand CP); in case (ii), $\boldsymbol{E}_\parallel$ and $\boldsymbol{E}_\perp$ oscillate 180° out of phase (they have opposite signs), and the tip of the vector sum of $\boldsymbol{E}_\parallel$ and $\boldsymbol{E}_\perp$ moves in the clockwise (CW) direction on the sky, corresponding to negative CP (left-hand CP). Cases (iii) and (iv) are entirely analogous to cases (i) and (ii).

3 HELICAL *B* FIELDS AND CONVERSION

As has been mentioned by Wardle & Homan (2002) and analysed in more detail by Ensslin (2003), a helical jet $\boldsymbol{B}$ field geometry can facilitate the conversion process – a small fraction of the LP from the far side of the jet relative to the observer is converted to CP as it passes through magnetized plasma in or near the near side of the jet. The angle Φ – and thereby the distribution of CP – will vary across the jet, but in observations with limited resolution, the overall observed CP sign should correspond to that near the central axis, provided that the overall jet $\boldsymbol{B}$ field is dominated by the ordered helical component rather than a chaotic component. The observed CP sign and distribution will also be affected by the viewing angle; however, we are viewing the jets of radio-bright AGN at angles close to 90° in the jet rest frame ($\simeq 1/\Gamma$ in the observer's frame, where Γ is the bulk Lorentz factor for the jet; e.g. Lyutikov, Pariev & Gabuzda 2005; Cohen et al. 2007), so that this effect should not radically change the observed picture. In the absence of other propagation effects, such as Faraday rotation of the plane of polarization, the sign of the generated CP is determined by the pitch angle ψ (the angle between $\boldsymbol{B}$ and the helix axis projected on to the sky) and the helicity of the jet $\boldsymbol{B}$ field. Table 1 summarizes the CP sign obtained for conversion in a simple hollow helical field with pitch angle ψ and a specified helicity. These pitch angles correspond to the case when the longitudinal $\boldsymbol{B}$ field component points along the jet; if this component points opposite to the jet, the effective pitch angle will be greater than 90°, and the CP sign for a pitch angle of $180 - \psi$ will be the same as that for ψ with the same helicity. We will return to this question below.

Thus, if we are able to determine both the helicity and pitch-angle regime for a helical $\boldsymbol{B}$ field associated with a particular AGN jet, the sign of the CP generated by Faraday conversion in this helical field can be predicted.

Table 1. CP signs for conversion in helical fields.

Pitch angle	Helicity	Φ range	CP sign
$0^\circ < \psi < 45^\circ$	Right-hand	$0^\circ < \Phi < 90^\circ$	+
$45^\circ < \psi < 90^\circ$	Right-hand	$90^\circ < \Phi < 180^\circ$	−
$45^\circ < \psi < 90^\circ$	Left-hand	$180^\circ < \Phi < 270^\circ$	+
$0^\circ < \psi < 45^\circ$	Left-hand	$270^\circ < \Phi < 360^\circ$	−

3.1 Estimating the *B* field pitch angle

The approximate pitch angle of a helical $\boldsymbol{B}$ field associated with an AGN jet is indicated by the dominant LP structure. The observed plane of polarization will be essentially orthogonal to the synchrotron $\boldsymbol{B}$ field in the optically thin jets: helical fields with relatively large/small pitch angles will tend to be dominated by the toroidal/longitudinal components of their helical fields. Thus, fields with *large* pitch angles should tend to have 'transverse' $\boldsymbol{B}$ fields or a central 'spine' of transverse field with a 'sheath' of longitudinal field at one or both edges of the jet, while fields with small pitch angles should tend to have longitudinal $\boldsymbol{B}$ fields throughout the jet. Although the observed $\boldsymbol{B}$ field structure is also affected by the viewing angle, recall that we are viewing these jets roughly 'side-on' in the jet rest frame, so that the above tendencies should, in general, be obeyed.

3.2 Determining the *B* field helicity

If a jet has a helical $\boldsymbol{B}$ field and there is thermal plasma in the jet or its immediate vicinity, we will observe an RM gradient across the jet, due to the systematically changing line-of-sight component of the helical $\boldsymbol{B}$ field (Blandford 1993). The observed RMs will have opposite signs at opposite edges of the jet when the viewing angle is close to 90° to the jet axis in the jet rest frame (close to $1/\Gamma$ in the observer's frame), while the RM range may encompass RM values of only one sign when the viewing angle differs appreciably from this value. Such transverse RM gradients have been observed for a number of AGN (Asada et al. 2002; Gabuzda, Murray & Cronin 2004; Zavala & Taylor 2005), and several more are reported here. Note that Sikora et al. (2005) have pointed out that the observation of Faraday rotations exceeding approximately 45° in some cases indicates that the Faraday rotation has to be external, suggesting that it is occurring in outer layers of the jet flow rather than throughout the jet volume.

The helicity of the jet $\boldsymbol{B}$ field is directly related to the direction of the RM gradient. However, an ambiguity arises when we try to deduce the helicity based on an observed transverse RM gradient. As is shown in Fig. 2, a right-handed helix with an 'inward' ('south') poloidal component will display the same sense of RM gradient as a left-handed helix with an 'outward' ('north') poloidal component. None the less, the two cases could, in principle, be distinguished observationally because they will give rise to different signs of CP, due to their different helicities.

4 THE DATA AND THEIR REDUCTION

We have identified eight AGN for which (i) parsec-scale CP has been detected, (ii) transverse RM gradients have been detected and (iii) the LP structure is clear enough to be reasonably certain about the correct inferred jet $\boldsymbol{B}$ field structure: 0735+178, 1156+295, 3C 273, 3C 279, 1641+399 (3C 345), 1749+096, 2230+114 and 2251+158 (3C 454.3).

Five of these eight AGN appear in this list due to the new detections of transverse RM gradients (0735+178, 1156+295 and 1749+096) and CP (3C 345 and 2231+114) reported here. In all cases, the target sources were observed in a 'snapshot' mode, with typically 8–10 scans of each object spread out over the time the source was visible with most or all of the VLBA antennas. The data reduction and imaging were done in the AIPS package using standard techniques. The instrumental polarizations ('D-terms') were

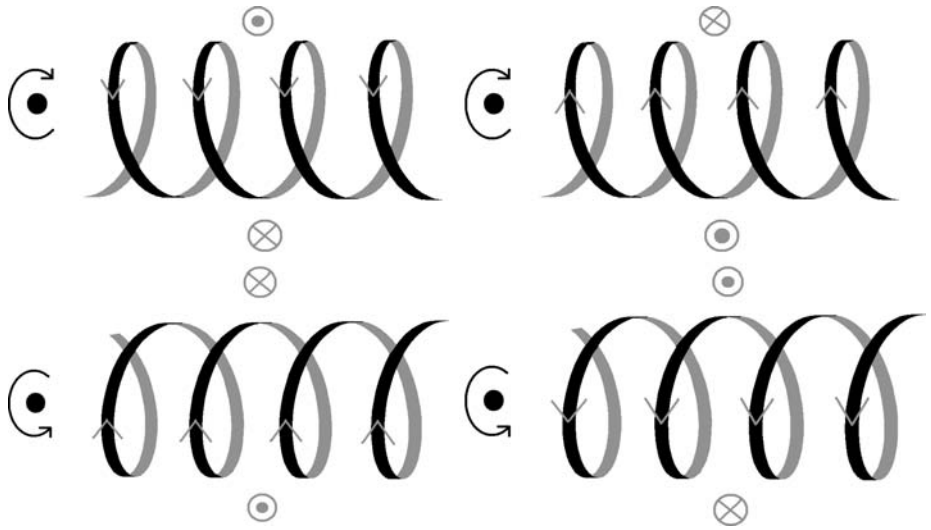

Figure 2. Diagrams showing the senses of the transverse Faraday-rotation gradients brought about by a jet $\boldsymbol{B}$ field in the form of a right-handed (top) and left-handed (bottom) helix with poloidal component oriented away from (left-hand diagram) and towards (right-hand diagram) the central black hole, which is located in all cases to the left-hand side of the region shown. The direction of the rotation of the central black hole/accretion disc is also indicated to the left-hand side. A circled dot indicates that the toroidal component of the field is pointed towards the observer, and a circled cross that this component is pointed away from the observer.

determined using the AIPS task LPCAL, solving simultaneously for the source polarization.

The calibration of the absolute electric vector position angles (EVPAs) was determined using integrated polarization measurements obtained using the Very Large Array near in time to our observations (www.aoc.nrao.edu/smyers/calibration/), by requiring that the EVPA for the total VLBI polarization of compact sources coincide with the EVPAs for their VLA cores. We estimate that our overall EVPA calibration is accurate to within about 3°. The rms noises in the maps of the Stokes parameters Q and U were used to estimate the uncertainties in the VLBA polarization angles χ in each pixel of the χ maps. Note that any errors in the EVPA calibration affect all polarization angles in all regions of all the sources in the same way, and so could hinder the detection of Faraday-rotation gradients, but will not lead to the presence of spurious Faraday-rotation gradients in the source structure.

4.1 Faraday-rotation observations

The polarization observations used for our Faraday-rotation measurements were obtained on 2003 August 22 (1156+295), 2004 March 22 (1749+096) and 2004 September 10 (0735+178) at 15.1, 12.9, 8.6, 7.9, 5.1 and 4.6 GHz using the NRAO VLBA. The polarization D-terms were derived from observations of DA193 (2003 August), 0235+164 (2004 March) and 1732+389 (2004 September).

We made maps of the distribution of the Stokes parameters Q and U with matched resolutions corresponding to the 4.6- or 8.1-GHz beam (indicated in a corner of the map figures). The Q and U maps were than used to construct the distributions of the polarized flux ($p = \sqrt{Q^2 + U^2}$) and polarization angle [$\chi = (1/2)\arctan(U/Q)$], as well as accompanying 'noise maps', using the AIPS task COMB. The formal uncertainties written in the output χ noise maps were calculated in COMB using the rms noise levels on the input Q and U maps.

The RM maps were constructed as is described by Gabuzda et al. (2004), using χ maps with matched beam sizes at the six frequencies. We removed the contributions of the known integrated (predominantly Galactic, i.e. foreground; Pushkarev 2001) Faraday rotations at each frequency before making the RM maps, so that any remaining rotation measures should be due to thermal plasma in the vicinity of the AGN. The AIPS task RM has the option of blanking output pixels when the uncertainty in the RM exceeds a specified value; the maximum allowed RM uncertainties are indicated in the caption to Fig. 3.

When determining the χ values for individual regions in the VLBI jet, we found the mean within a 3 × 3 pixel (0.3 × 0.3 mas) area at the corresponding location in the map; the polarization angles were assigned errors equal to the rms deviation for this mean value and the estimated EVPA calibration uncertainty of 3° added in quadrature.

4.2 VLBA CP observations

The VLBA observations of 10 AGN used in our CP analysis were obtained at 15.3 GHz on 2004 November 1. The polarization D-terms were derived from observations of 1156+295.

The CP calibration of the gains was done using the well-established gain-transfer technique of Homan & Wardle (1999), described in detail both in that paper and by Vitrishchak & Gabuzda (2007). CP was detected in three of the ten AGN observed: 1633+283, which was found to have a CP of (-0.23 ± 0.06) per cent, consistent with the value of (-0.39 ± 0.09) per cent reported by Homan & Lister (2006), and 1641+399 ($+0.15 \pm 0.06$ per cent) and 2230+114 (-0.47 ± 0.12 per cent), for which we report the first CP detections here. A table of all the CP measurements for our 2004 November 1 15.3-GHz data are given in Table 2. The 1σ uncertainties in the CP values were determined in the same way as is described by Homan et al. (2001), including contributions for uncertainty (i) in the smoothed antenna gains, (ii) due to real CP in the calibrators and (iii) due to random scan-to-scan gain variations. In the case of non-detections, the presented upper limits are the corresponding 1σ uncertainties. The uncertainty-estimation procedure used is relatively conservative, and we are in the course of investigating a Monte Carlo approach to estimating the CP uncertainties, similar to that used by Homan & Lister (2006).

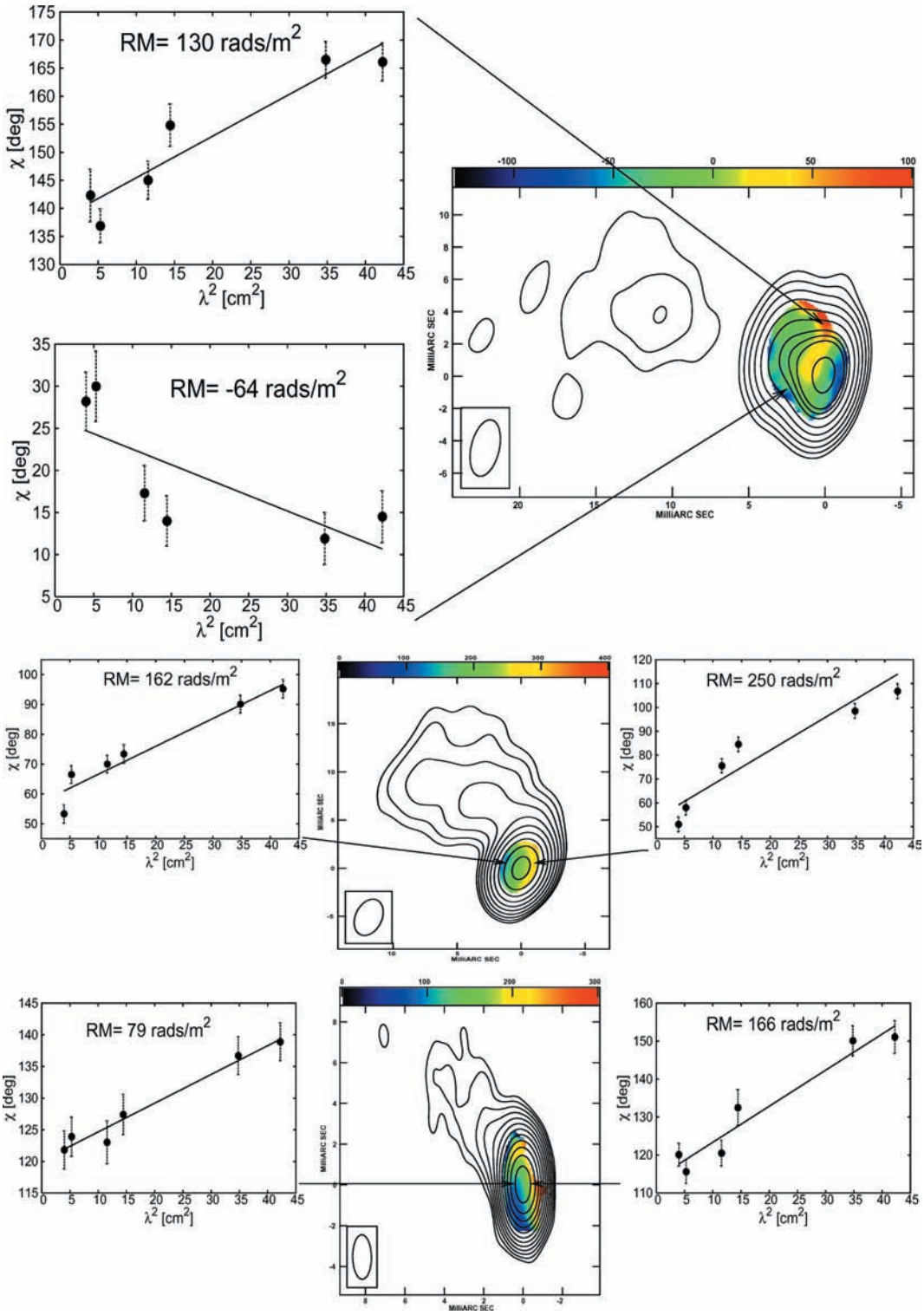

Figure 3. VLBA *I* maps of 0735+178 (top; 4.6 GHz; peak 0.62 Jy beam^{-1}; bottom contour 2.0 mJy beam^{-1}), 1156+295 (middle; 5.1 GHz; peak 1.32 Jy beam^{-1}; bottom contour 1.6 mJy beam^{-1}) and 1749+096 (bottom; 7.9 GHz; peak 3.30 Jy beam^{-1}; bottom contour 1.0 mJy beam^{-1}), with the parsec-scale RM distributions superimposed. In all cases, north is upward, east is to the left-hand side and the contours increase in steps of a factor of 2. The accompanying graphs show plots of χ (in degrees) versus λ^2 (in cm^2) for locations on opposite sides of the VLBI jets, with χ errors of 1σ. The convolving beams are shown in the bottom right-hand corner of the maps. The maximum allowed uncertainty in the RM values per pixel were 30 rad m^{-2} for 0735+178, 10 rad m^{-2} for 1156+295 and 25 rad m^{-2} for 1749+096.

Table 2. 15.3-GHz CP results for 2004 November 1.

Source	Alias	I peak (Jy)	m_c (per cent)	σ
0048−097		0.55	<0.12	–
0256+075		0.22	<0.18	–
0804+499		0.56	<0.07	–
0906+430		0.66	<0.08	–
1156+295		0.48	<0.08	–
1633+382		2.63	-0.23 ± 0.06	3.8
1641+399	3C 345	1.98	$+0.15 \pm 0.06$	2.5
2134+004		0.91	<0.13	–
2230+114	CTA102	1.06	-0.47 ± 0.12	3.9

5 RESULTS

Fig. 3 shows the VLBI I images of 0735+178, 1156+295 and 1749+096 with colour images of their parsec-scale RM distributions superposed. The convolving beams used in each case are indicated in the lower right-hand corner of the figure. The RM gradients across the VLBI jets are visible by eye. The accompanying plots show the observed polarization position angles, χ, as a function of the observing wavelength squared, λ^2, for individual locations in the VLBI jets, with 1σ errors in χ.

The observed total-intensity and linear polarization (LP) structures for each of the eight objects listed above at the first MOJAVE epoch are presented by Lister & Homan (2005); additional images for other epochs are available at the site http://www.physics.purdue.edu/astro/MOJAVE/. We present the total-intensity and LP structures for the five of these eight objects for which we have reported new transverse RM gradients or CP measurements in Figs 4 and 5.

Let us briefly discuss the ***B*** field structures we infer from the LP structure of each of the eight sources considered here (for the purpose of determining the approximate pitch angles of the helical ***B*** fields associated with their jets). Note that the Faraday rotations in the central regions of the jets typically produce rotations of no more than 5°–10° at the wavelengths considered here, so that this does not drastically affect our ability to draw conclusions about the jet ***B*** field structures.

0735+178: This BL Lac object has been analysed in detail in a number of VLBI studies (Gabuzda et al. 1994; Gabuzda, Gómez & Agudo 2001; Gómez et al. 2001; Agudo et al. 2006). In some time intervals, the VLBI jet has appeared relatively straight, while in others, it has shown an unusual 'zig-zag' structure, with two sharp bends in the inner jet. The MOJAVE maps and our own image in Fig. 4 may correspond to a transition from the zigzag to a straighter jet structure (Agudo et al. 2006), but the origin of this transition (e.g. changes in the projected bends on the plane of the sky, changes in the physical structure of the jet itself) is not entirely clear. Our image seems to indicate a predominantly longitudinal jet ***B*** field (the polarization vectors lie perpendicular to the jet); however, the previous studies cited above have indicated a clear tendency for the dominant ***B*** field in the inner jet to be *orthogonal* to the jet. Fig. 4 also shows the first-epoch MOJAVE images of 0735+178, which, like our own image, seem to display an extended region of longitudinal field in the outer jet, but also clearly show a region in the core/inner jet which has a transverse ***B*** field. Overall, given that earlier images have shown clear evidence for a predominant transverse jet ***B*** field in the inner jet and there have been dramatic changes in the observed jet structure, we suggest that the extended regions of longitudinal field indicated by the maps in Fig. 4 may reflect interactions between the jet and the surrounding medium, rather than the intrinsic pitch angle of the helical jet ***B*** field. Thus, although this is a somewhat problematic case, we have taken the predominant intrinsic jet ***B*** field in 0735+178 (i.e. that field that reflects the pitch angle of the helical field) to be orthogonal to the jet.

1156+295: The VLBI jet of 1156+295 initially emerges nearly due north, then curves to the east. Our image in Fig. 5 shows a clear spine + sheath type structure in the LP, with the inferred ***B*** field perpendicular to the jet near the jet axis and longitudinal to the jet near its edges, consistent with the MOJAVE polarization images. Polarization observations of 1156+295 at 15, 8.4 and 5 GHz obtained in 2005 September show a very similar polarization structure, and also confirm the presence of a transverse RM gradient with the same sense (Gabuzda, Mahmud & Kharb, in preparation).

3C 273: A number of polarization studies have been devoted to this well-known quasar; it was the first AGN for which a transverse RM gradient indicative of a helical ***B*** field was reported, by Asada et al. (2002), subsequently confirmed by Zavala & Taylor (2005) and Attridge, Wardle & Homan (2005). The dominant inferred ***B*** field is longitudinal throughout the observed jet, including the smallest scales probed by 43-GHz VLBA observations (Jorstad et al. 2005).

3C 279: This object has also been included in many studies; in addition, it is often observed as a calibrator due to its brightness, compactness and the relative stability of its polarization angles. The MOJAVE images show that the dominant ***B*** field is orthogonal to the jet throughout the observed jet, and this tendency is retained on the smallest scales probed by 43-GHz VLBA observations (Jorstad et al. 2005).

1641+399 (3C 345): A number of polarization studies have been devoted to this well-known quasar (e.g. Ros, Zensus & Lobanov 2000, and references therein). It is one of only a few AGN for which there is firm evidence that different jet components have been ejected in different structural position angles, and follow different trajectories, which ultimately merge to form the more outer VLBI jet. Although individual components with ***B*** fields orthogonal to the jet have been detected in the innermost jet, these may be associated with shocks; the predominant jet ***B*** beyond 1–2 mas from the core has consistently been observed to be longitudinal, and we accordingly adopt this latter field as the ***B*** field that should be used to deduce the pitch-angle regime.

1749+096: This very compact BL Lac object was included in a number of earlier studies (e.g. Gabuzda et al. 2000, and references therein; Gabuzda 2003), and in all cases the dominant ***B*** field has been orthogonal to the jet. Our new 5.1-GHz image in Fig. 4 displays such an orthogonal field in the inner part of the jet, possibly with signs of a spine + sheath like structure appearing further from the core. The 15.4-GHz MOJAVE image likewise clearly shows a region of transverse ***B*** field in the inner jet, to the north of the core; the jet makes a sharp turn to the east, and the polarization sticks in this more extended region remain aligned with the new jet direction. A hint of a transverse RM gradient in 1749+096 with the same sense as the one shown in Fig. 3 is visible in the RM map of Zavala & Taylor (2004).

2230+114: The behaviour of this AGN is similar to that of 3C 345: close to the VLBI core, there is a compact region whose polarization is sometimes aligned with or oblique to the jet direction, while the predominant ***B*** field beyond 1–2 mas is clearly longitudinal (e.g. Fig. 5). Again, based on its stability in time, we adopt the longitudinal field as the ***B*** field that should be used to deduce the pitch-angle regime.

2251+158 (3C 454.3): The VLBI jet of this well-known quasar is very complex, but the MOJAVE polarization images

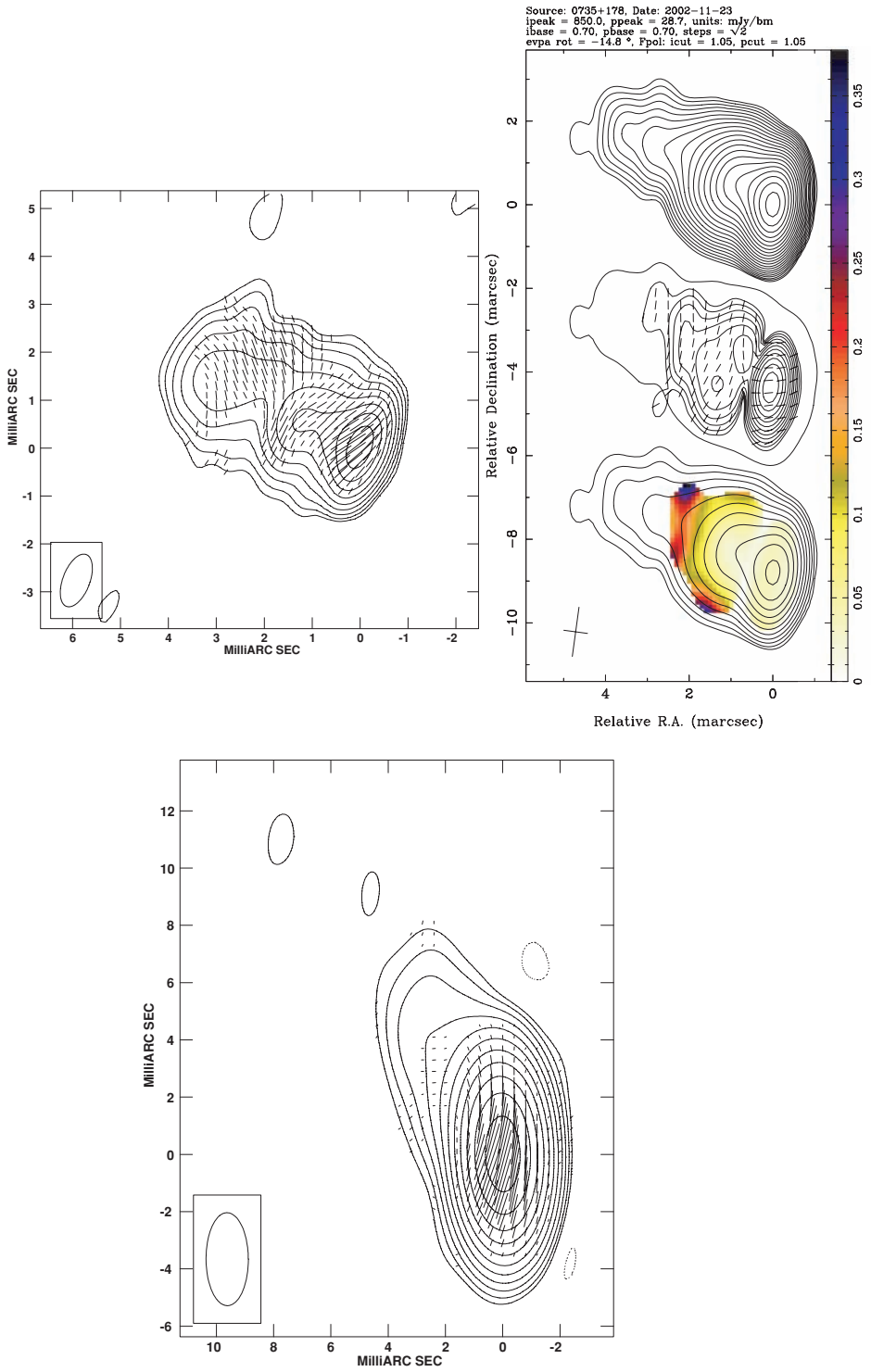

Figure 4. Top left-hand panel: VLBA *I* map of 0735+178 with polarization sticks superimposed from our data obtained on 2004 September 10 at 15.1 GHz (peak 0.45 Jy beam^{-1}; bottom contour 1.1 mJy beam^{-1}; contour step of two). Top right-hand panel: VLBA *I* map (peak 0.85 Jy beam^{-1}; bottom contour 0.70 mJy beam^{-1}; contour step of $\sqrt{2}$), polarized flux map with polarization sticks superimposed and *I* map with the distribution of the degree of polarization superimposed at the first MOJAVE epoch on 2002 November 23 at 15.4 GHz. The predominance of a transverse ***B*** field in the core region at the MOJAVE epoch is clearly visible. Bottom: VLBA *I* map of 1749+096 with polarization sticks superimposed from our 5.1-GHz data obtained on 2004 March 22 (peak 2.21 Jy beam^{-1}; bottom contour 1.4 mJy beam^{-1}; contour step of 2); the polarization structure shown in the first-epoch MOJAVE data obtained on 2002 May 31 is similar. The convolving beams are shown in the bottom right-hand corner of the maps.

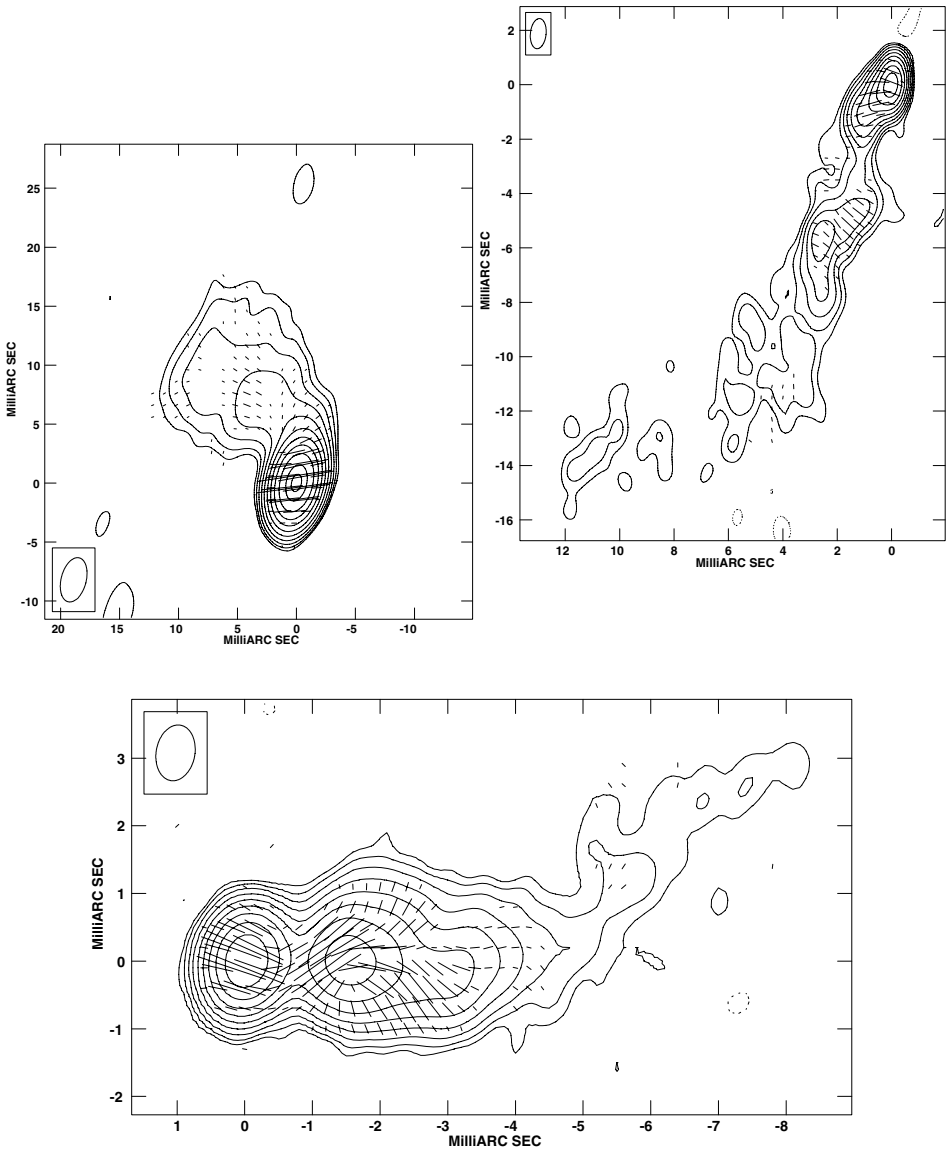

Figure 5. VLBA *I* maps with polarization sticks superimposed at 5.1 GHz at epoch 2003 August 22 for 1156+295 (top left-hand panel; peak 1.32 mJy beam^{-1}; bottom contour 1.6 mJy beam^{-1}), and at 15.3 GHz at epoch 2004 November 1 for 2230+114 (top right-hand panel; peak 1.06 mJy beam^{-1}; bottom contour 2.7 mJy beam^{-1}) and 1641+399 (bottom; peak 1.98 mJy beam^{-1}; bottom contour 4.2 mJy beam^{-1}). In all cases, the contours increase in steps of a factor of 2. The convolving beams are shown in some corner of the maps.

display a clear spine + sheath structure, and the orthogonal $\boldsymbol{B}$ field near the central ridge line of the jet clearly dominates at higher frequencies (Jorstad et al. 2005).

Table 3 summarizes the $\boldsymbol{B}$ field structures, pitch-angle regimes implied by these $\boldsymbol{B}$ field structures ['small' $= 0^\circ < \psi < 45^\circ$ and 'large' $= 45^\circ < \psi < 90^\circ$], helicities implied by the observed transverse RM gradients for the case of north and south poloidal magnetic field components $\boldsymbol{B}_{\rm pol}$ and the expected CP signs for each of these two cases. This table also presents the observed parsec-scale CP values. *In all eight AGN, the observed sign of the CP agrees with the sign expected for our simple helical-field model for the case of a south poloidal field.* This clearly non-random pattern of agreement between the expected and observed CP signs represents powerful evidence that the detected CP is generated by Faraday conversion in the helical jet $\boldsymbol{B}$ fields of these objects, accompanied by unexpected evidence that the poloidal fields in the jets preferentially correspond to south polarity.

If the detected CP had no connection with the presence of helical fields, the predicted and observed CP signs should agree and disagree in roughly half the cases for each sense of the poloidal magnetic field. Testing this hypothesis using the binomial probability distribution, specifying equal probabilities for the expected and observed CP signs agreeing or disagreeing, yields a probability of only 0.4 per cent that the perfect agreement between our predicted CP signs for the case of south poloidal field and the observed CP signs came about purely by chance.

6 DISCUSSION

6.1 Location of detected CP in the VLBI cores

It is important to note that the 'core' as the optically thick base of the jet (Blandford & Königl 1979) is a theoretical concept, and will correspond to the observed 'core' only for observations with sufficient

Table 3. AGN jets with transverse RM gradients and CP.

Source	Dominant jet $\boldsymbol{B}$ field[a]	Pitch angle regime	Helicity (north $\boldsymbol{B}_{\rm pol}$)	Expected CP sign	Helicity (south $\boldsymbol{B}_{\rm pol}$)	Expected CP sign	Observed CP (per cent)	Implied $\boldsymbol{B}_{\rm pol}$	CP reference	RM reference
0735+178	$\perp$	Large	Left-hand	+	Right-hand	−	-0.30 ± 0.11	S	1	*
1156+295	SS	Large	Left-hand	+	Right-hand	−	-0.27 ± 0.09	S	1	*
3C 273	$\parallel$	Small	Right-hand	+	Left-hand	−	-0.45 ± 0.09	S	1	3, 4
3C 279	$\perp$	Large	Left-hand	−	Right-hand	+	$+0.30 \pm 0.08$	S	1	5
3C 345	$\parallel$	Small	Left-hand	−	Right-hand	+	$+0.17 \pm 0.10$	S	*	6
1749+096	$\perp$	Large	Left-hand	+	Right-hand	−	-0.32 ± 0.13	S	2	*
2230+114	$\parallel$	Small	Right-hand	+	Left-hand	−	-0.48 ± 0.11	S	*	7
2251+158	SS	Large	Right-hand	−	Left-hand	+	$+0.23 \pm 0.10$	S	1	8

[a] $\perp$ = transverse, $\parallel$ = longitudinal, SS = spine + sheath.
References: (1) Homan & Lister (2006); (2) Vitrishchak & Gabuzda (2007); (3) Asada et al. (2002); (4) Zavala & Taylor (2005); (5) Zavala & Taylor (2004); (6) Taylor (1998); (7) Taylor (2000); (8) Zavala & Taylor (2003); (*) this paper.

resolution; the observed VLBI 'core' will actually correspond to a combination of the genuine optically thick core and optically thin emission from the inner jet. Taking this into account, in our model, the fact that the detected CP usually coincides with the VLBI 'core' is essentially a selection effect. The Faraday conversion occurs to some extent on all scales in the jets, including on smaller scales than the resolution of the VLBI observations, and it is natural that the inner jet dominates the CP signal, since this is the brightest part of the jet. In addition, this effect may be enhanced by the fact that the $\boldsymbol{B}$ field strengths and (thermal) plasma densities that determine the conversion may rise towards the active nucleus of the AGN.

It is interesting that CP has, in fact, been directly detected in the VLBI *jets* of seven AGN (Homan & Lister 2006; Vitrishchak & Gabuzda 2007), three of which appear in Table 2 (3C 273, 3C 279, 2252+158). Of these seven AGN, all but 3C 84, which is clearly an unusual object (Homan & Wardle 2004), display extended regions of CP of a single sign. This behaviour is fully consistent with the CP being associated with a helical jet $\boldsymbol{B}$ field whose pitch angle and helicity determine the sign of the observed CP.

6.2 Sensitivity of results to viewing angle

We have carried out the above analysis assuming that we view most AGN jets at angles not very different from $1/\Gamma$ (90° in the jet rest frame). For example, the analysis of Cohen et al. (2007) suggests that the most likely angle to the line of sight is approximately $0.6/\Gamma$ ($\simeq 60^\circ$–65° in the jet rest frame for typical values of Γ). One natural question is how sensitive our results are to this assumption. In other words, for how large a range of angles do we expect to observe the CP sign predicted for a viewing angle of $\simeq 90^\circ$ in the jet rest frame?

To address this question in a first approximation, we have constructed two-dimensional plots of the expected CP sign for a hollow, right-handed helical $\boldsymbol{B}$ field as a function of distance from the jet axis and viewing angle in the jet rest frame, shown in Fig. 6. Note that there is some physical basis for adopting such a model, since the thermal plasma giving rise to the transverse RM gradients appears to be external to the bulk of the jet volume in at least some cases (Sikora et al. 2005). In Fig. 6, the distance from the jet axis is indicated in arbitrary units, with 0 corresponding to the position of the jet axis ('spine') and ± 1 corresponding to the two edges of the jet. Regions of positive CP are coloured red and regions of negative CP blue. Regions predicted not to give rise to CP because the projected angle between the background and foreground fields is 0° or a multiple of 90° are white, while regions corresponding to the intermediate 'optimal' angles for generating CP via Faraday conversion, near odd multiples of 45°, are coloured most intensely. These diagrams are calculated based purely on the angle between the background field $\boldsymbol{B}_{\rm gen}$ and foreground field $\boldsymbol{B}_{\rm conv}$ for a helical field with pitch angle ψ as seen by an observer viewing the jet at an angle θ projected on to the sky (this formula corresponds to a right-handed helix; in the analogous expression for a left-handed helix, the pitch angle ψ is replaced by $-\psi$):

$$\Phi = 2 \arctan \left[\frac{\sqrt{1-x^2} \sin \psi}{\sin\theta \cos\psi - x \cos\delta \sin\psi} \right].$$

Thus, it is important to bear in mind that they do not represent the actual intensity of the CP, merely the sign that should be produced for a specified viewing angle, pitch angle and relative distance from the jet axis. For comparison, we also show the CP sign distribution across the jet as a function of viewing angle for a pitch angle of 70° and a left-handed helical field. Note that, in this simple treatment, these images are point-symmetric.

While these diagrams do not take into account a number of potentially significant effects, such as effects due to the propagation of the synchrotron radiation emitted at the 'back' of the jet along the line of sight through the jet volume on its way to the observer, they nevertheless provide a useful overview of the expected robustness of our approach. We plan in future to carry out more complete radiative-transfer calculations of the expected CP distributions across the jet as a function of pitch angle and viewing angle.

The approach we have used will be relatively robust if the predicted CP sign is constant over a large fraction of the jet cross-section and for a fairly wide range of viewing angles. We can see that this will be the case for essentially all pitch angles that are not too close to those values that yield zero CP. There is an interesting selection effect here that helps make our approach relatively robust – the pitch angles for which there is a relatively small range of viewing angles corresponding to the CP sign observed for a viewing angle of 90° in the jet frame are also those that give rise to relatively weak CP. Thus, given the weakness of the CP signal, the AGN from which we detect parsec-scale CP will tend to be those with jets whose pitch angles are far from these values, so that the inferred CP sign is constant over a wide range of viewing angles.

6.3 Expected overall robustness of the approach

Despite the success of our approach for the eight AGN considered here, there are limitations to its robustness. We argue above that the dependence of the CP sign on the viewing angle is not likely to play the most important role. We note as well that this first simple

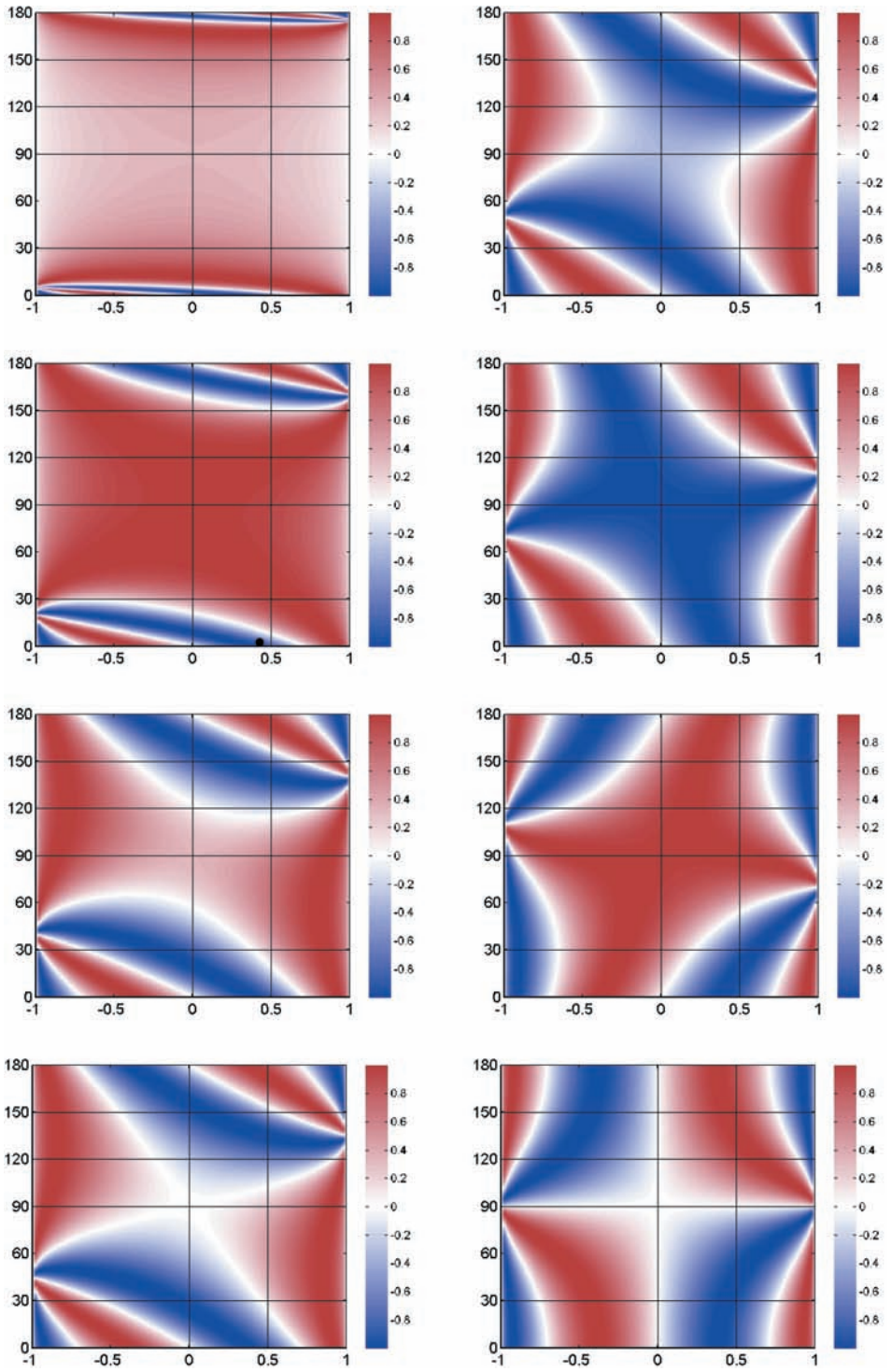

Figure 6. Diagrams showing the sign of CP generated by Faraday conversion in a helical jet $\boldsymbol{B}$ field as a function of the relative location across the jet (horizontal axis running from -1 at left-hand panels to $+1$ at right-hand panels, 0 corresponds to the 'spine' of the jet) and the angle at which the jet is viewed in the jet rest frame (vertical axis running from 0° at bottom to 180° at top; 0°, 90° and 180° correspond to an observer viewing the jet 'head-on', 'side-on' and 'tail-on', respectively). The left-hand column shows diagrams for right-handed helices with pitch angles 5°, 20°, 40° and 45° (top to bottom), while the right-hand column shows diagrams for right-handed helices with pitch angles of 50° and 70°, a left-handed helix with pitch angle 70° and the limiting case of a right-handed helix with pitch angle 90°. Red and blue correspond to positive and negative CP.

analysis has not included the effects of possible modest Faraday rotation in the jet volume, which will affect the angle between the polarization $\boldsymbol{E}$ vector and conversion $\boldsymbol{B}$ field. However, the weakest link in the procedure we have outlined is probably inferring the pitch-angle regime for the helical jet $\boldsymbol{B}$ field based on the observed polarization structure. In particular, there are other physical mechanisms that could give rise to a predominance of orthogonal or longitudinal $\boldsymbol{B}$ fields in AGN jets. Orthogonal fields can be

generated by shock compression, and the longitudinal $\boldsymbol{B}$ field component may be enhanced during shear interactions between the jet and the medium through which it flows. If one or both of these mechanisms operate, the associated $\boldsymbol{B}$ field structure will be superposed on the 'intrinsic' $\boldsymbol{B}$ field structure associated with the helical field, possibly leading to incorrect conclusions about the pitch-angle regime for the helical field. However, the fact that our approach also requires that there be a transverse RM gradient across the jet, thereby providing direct evidence for a predominant helical $\boldsymbol{B}$ field, may help reduce ambiguity in the inferred pitch-angle regime due to these effects.

6.4 Implications of results for the jet 'seed' field

As is shown in Fig. 2, a right-handed helix with a south poloidal component will display the same sense of RM gradient as a left-handed helix with a north poloidal component. This means, for example, that the helicity we would infer in this case based on the observed transverse RM gradient would be incorrect if we assumed the jet base represented a *north* magnetic pole, but in fact it represented a *south* pole.

Therefore, if statistically equal numbers of the approaching jets in the eight AGN considered here corresponded to north and south magnetic poles, the sense of the poloidal fields that yielded agreement between the predicted and observed CP signs would have been north in roughly half the cases and south in roughly half the cases. Since we have no other way to verify the sense of the poloidal field observationally, it would not have been possible to draw conclusions about whether, in fact, conversion in a helical-field geometry was the origin of the observed CP. However, our expected CP signs for south poloidal fields matched the observed values in eight out of eight cases; the probability of this happening just by chance is less than 1 per cent (it is equivalent to the probability of flipping a coin eight times and getting 'heads' all eight times).

This leads us to conclude that our results provide evidence for a predominance of south poloidal components among the jet $\boldsymbol{B}$ fields. This does not seem plausible if the seed fields that are transformed into a helical-like field by the jet outflow and rotation of the central objects are essentially dipolar. In this case, each black hole would have one jet with a north poloidal field and one with a south poloidal field, which should be randomly oriented in space, so that there are equal probabilities that the approaching jet corresponds to the south and north poles of the black hole. However, another possibility is that the seed field generated by the rotating central black hole is actually quadrupolar-like, with two north poles or two south poles, such that the magnetic field lines close through the equatorial plane. In fact, it has recently been suggested that such a quadrupolar $\boldsymbol{B}$ field may more likely be realized for black holes/accretion disc systems in AGN than a dipolar field (Blandford 2008). Our results would be consistent with this type of initial $\boldsymbol{B}$ field configuration if there were some reason for a predominance of quadrupolar initial $\boldsymbol{B}$ field configurations with two south poles, rather than two north poles. At present, however, we are not aware of any possible physical origin for such an asymmetry.

7 CONCLUSION

Despite extensive analyses of the degree of CP in previous studies, we are the first to consider the *sign* of the parsec-scale CP of AGN. The new transverse Faraday-rotation gradient and parsec-scale CP detections reported here have enabled us to compile a list of eight AGN with both CP detections and direct evidence for helical jet $\boldsymbol{B}$ fields. The perfect agreement between the observed CP signs and the CP signs expected if the CP is generated by Faraday conversion in helical jet fields whose poloidal component is oriented opposite to the jet conclusively demonstrates that the observed CP is intrinsically related to the helical jet $\boldsymbol{B}$ fields in these objects. Although the possibility of conversion-generated CP has been considered in a number of theoretical studies, this represents the first direct *observational* evidence pointing towards this specific CP-generation mechanism in the more than three decades since the earliest studies of CP in AGN.

This result has far-reaching implications for our understanding of the processes occurring in AGN jets, since it suggests that helical jet $\boldsymbol{B}$ fields are common in AGN, possibly even ubiquitous. Indeed, such helical $\boldsymbol{B}$ fields can be produced very naturally through the 'winding up' of a seed field by rotation of the central black hole and accretion disc, combined with the jet outflow (e.g. Meier, Koide & Uchida 2001; Kato, Mineshige & Shibata 2004; McKinney 2006). The generation of a helical field requires the presence of a significant poloidal field, which can come about due to the jet outflow. The presence of helical jet $\boldsymbol{B}$ fields provides a means to collimate the jets, and demands that the jets carry current (e.g. Lovelace et al. 2002; Tsinganos & Bogovalov 2002). Thus, it is clear that we must view AGN jets as fundamentally electromagnetic structures, although it is less clear from the available observations whether or not the jets are actually dynamically dominated by the associated electromagnetic forces.

Our results also appear to provide evidence that the initial 'seed' fields of the central black holes are typically quadrupolar rather than dipolar, with a predominance of quadrupolar fields with two south poles. Numerical simulations of the joint action of rotation and outflow on an initial quadrupolar field would be helpful in determining if there is a theoretical basis for this possible asymmetry between these two field configurations. An interesting observational distinction between dipolar and quadrupolar field configurations for the central black holes was recently pointed out by Blandford (2008): in the case of a helical jet $\boldsymbol{B}$ field generated from a dipolar seed field, the transverse Faraday-rotation gradients for the approaching jet and receding counterjet should have *opposite* directions, while these two gradients will be in the *same* direction if the seed field that is 'wound up' by the rotation of the system is quadrupolar. The observational challenge is therefore to identify AGN in which both total intensity and polarization are detected in both the jet and counterjet on scales on which the transverse Faraday-rotation gradients due to the helical jet $\boldsymbol{B}$ fields are reliably detected, and to carry out sensitive Faraday-rotation measurements for such objects (the apparent absence of clear RM gradients in FRI jets on kiloparsec scales (e.g. Laing & Bridle 2008) may indicate that the systematic transverse RM gradients are disrupted by chaotic or turbulent motions on these scales).

We plan to analyse multiwavelength VLBA polarization observations for several additional AGN with detected parsec-scale CP in order to search for transverse Faraday-rotation gradients in these objects, with the aim of further investigating the relationship between the LP structures, $\boldsymbol{B}$ field helicities and observed CP in AGN. We also plan to consider the possible influence of modest amounts of Faraday rotation on the observed CP in a future paper.

ACKNOWLEDGMENTS

We thank T. V. Cawthorne, D. Meier, N. O'Murchadha and J. F. C. Wardle for useful and interesting discussions of this work. We are also grateful to the referee, Thomas Beckert, for pertinent and

clearly explained comments that have appreciably improved this paper.

REFERENCES

Agudo I., Gómez J. L., Gabuzda D. C., Marscher A. P., Jorstad S. G., Alberdi A., 2006, A&A, 453, 477
Asada K., Inoue M., Uchida Y., Kameno S., Fijisawa K., Iguchi S., Mutoh M., 2002, PASJ, 54, L39
Attridge J. M., Wardle J. F. C., Homan D. C., 2005, ApJ, 633, L85
Beckert T., Falcke H., 2002, A&A, 388, 1106
Blandford R. D., 1993, Astrophysical Jets. Cambridge Univ. Press, Cambridge, p. 26
Blandford R. D., 2008, in Rector T., De Young D. S., eds, ASP Conf. Ser., Extra galactic Jets: Theory and Observations from Radio to Gamma-rays. Astron. Soc. Pac., San Francisco, in press
Blandford R. D., Königl A., 1979, ApJ, 232, 34
Cohen M. H., Lister M. L., Homan D. C., Kadler M., Kellermann K. I., Kovalev Y. Y., Vermeulen R. C., 2007, ApJ, 658, 232
Conway R. G., Gilbert J. A., Raimond E., Weiler K. W., 1971, MNRAS, 152, 1
Ensslin T. A., 2003, A&A, 401, 499
Gabuzda D. C., 2003, in Takalo L. O., Valtaoja E., eds, ASP Conf. Ser. Vol. 299, High-Energy Blazar Astronomy. Astron. Soc. Pac., San Francisco, p. 99
Gabuzda D. C., Pushkarev A. B., Cawthorne T. V., 2000, MNRAS, 319, 1109
Gabuzda D. C., Wardle J. F. C., Roberts D. H., Aller M. F., Aller H. D., 1994, ApJ, 435, 128
Gabuzda D. C., Gómez J. L., Agudo I., 2001, MNRAS, 328, 719
Gabuzda D. C., Murray É., Cronin P. J., 2004, MNRAS, 351, L89
Gilbert J. A., Conway R. G., 1970, Nat, 227, 585
Gómez J. L., Guirado J. C., Agudo I., Marscher A. P., Alberdi A., Marcaide J. M., Gabuzda D. C., 2001, MNRAS, 328, 873
Homan D. C., Lister M. L., 2006, AJ, 131, 1262
Homan D. C., Wardle J. F. C., 1999, AJ, 118, 1942
Homan D. H., Wardle J. F. C., 2004, ApJ, 602, L13
Homan D. C., Attridge J. M., Wardle J. F. C., 2001, ApJ, 556, 113
Jones T. W., 1988, ApJ, 332, 678
Jones T. W., O'Dell S. L., 1977, ApJ, 214, 522
Jorstad S. G. et al., 2005, AJ, 140, 1418
Kato Y., Mineshige S., Shibata K., 2004, ApJ, 605, 307
Komesaroff M. M., Roberts J. A., Milne D. K., Rayner P. T., Cooke D. J., 1984, MNRAS, 208, 409
Laing R. A., Bridle A. H., 2008, in Rector T., De Young D. S., eds, ASP Conf. Ser., Extra galactic Jets: Theory and Observations from Radio to Gamma-rays. Astron. Soc. Pac., San Francisco, in press
Legg M. P. C., Westfold K. C., 1968, ApJ, 154, 499
Lister M. L., Homan D. C., 2005, AJ, 130, 1389
Lovelace R. V. E., Li H., Koldoba A. V., Ustyugova G. V., Romanova M. M., 2002, ApJ, 572, 445
Lyutikov M., Pariev V., Gabuzda D. C., 2005, MNRAS, 360, 869
Macquart J.-P., Melrose D. B., 2000, ApJ, 545, 798
McKinney J. C., 2006, MNRAS, 368, 1561
Meier D. L., Koide S., Uchida Yu., 2001, Sci, 291, 84
Pacholczyk A. G., 1970, Radio Astrophysics. Freeman & Co., San Francisco
Pushkarev A. B., 2001, Astron. Rep., 45, 667
Rayner D. P., Norris R. P., Sault R. J., 2000, MNRAS 319, 484
Roberts J. A., Cooke D. J., Murray J. D., Cooper B. F. C., Roger R. S., Ribes J.-C., Biraud F., 1975, Aust. J. Phys., 28, 325
Ros E., Zensus J. A., Lobanov A., 2000, A&A, 354, 55
Sikora M., Begelman M. C., Madejski G. M., Lasota J.-P., 2005, ApJ, 625, 72
Taylor G. B., 1998, ApJ, 506, 637
Taylor G. B., 2000, ApJ, 533, 95
Tsinganos K., Bogovalov S., 2002, MNRAS, 337, 553
Vitrishchak M. V., Gabuzda D. C., 2007, Astron. Rep., 51, 695
Wardle J. F. C., Homan D. A., 2002, in Laing R. A., Blundell K. M., eds, ASP Conf. Ser. Vol. 250, Particles and Fields in Radio Galaxies. Astron. Soc. Pac., San Francisco, p. 152
Wardle J. F. C., Homan D. A., 2003, ApSS, 288, 143
Weiler K. W., de Pater I., 1983, ApJS, 52, 293
Weiler K. W., Wilson A. S., 1977, A&A, 58, 17
Zavala R. T., Taylor G. B., 2003, ApJ, 589, 126
Zavala R. T., Taylor G. B., 2004, ApJ, 612, 749
Zavala R. T., Taylor G. B., 2005, ApJ, 626, L73

This paper has been typeset from a TEX/LATEX file prepared by the author.